Journal of Nanobiotechnology

RESEARCH Open Access

RSL3-loaded nanoparticles amplify the therapeutic potential of cold atmospheric plasma

Xiaona Cao[1,2,3†], Mo Chen[1,2†], Tianxu Fang[1,2], Yueyang Deng[1,2], Li Wang[1,2], Hanwen Wang[1,2], Zhitong Chen[4,5] and Guojun Chen[1,2*]

Abstract

Cold atmospheric plasma (CAP) has exhibited exciting potential for cancer treatment. Reactive oxygen and nitrogen species (RONS), the primary constituents in CAP, contribute to cancer cell death by elevating oxidative stress in cells. However, several intrinsic cellular antioxidant defense systems exist, such as the glutathione peroxidase 4 (GPX4) enzyme, which dampens the cell-killing efficacy of CAP. RAS-selective lethal 3 (RSL3), also known as a ferroptosis inducer, is a synthetic GPX4 inhibitor. Therefore, we hypothesized that RSL3 can amplify CAP-induced cell death by inhibition of GPX4. In this study, we showed that RSL3 loaded in poly (ethylene glycol)-block-poly(lactide-co-glycolide) (PLGA-PEG) nanoparticles can enhance CAP-induced cell deaths in 4T1 tumor cells. Furthermore, the combination of CAP and RSL3 also promoted cancer immunogenic cell death (ICD), induced dendritic cell (DC) maturation, and macrophage polarization, initiating tumor-specific T-cell mediated immune responses against tumors. For in vivo application, RSL3@NP was co-delivered with CAP *via* injectable Pluronic hydrogel. In 4T1-bearing mice, hydrogel-mediated delivery of CAP and RSL3-loaded nanoparticles can effectively elicit potent anti-tumor immune responses and inhibit tumor growth.

Keywords Cold atmospheric plasma, Immunogenic cell death, Drug delivery, RSL3, Injectable hydrogel, Nanoparticles

Introduction

Plasma, acknowledged as the fourth fundamental state of matter alongside solid, liquid, and gas, represents an ionized gas containing charged species, free electrons, and free radicals [1–4]. Given the progress in plasma technology, the spotlight has turned towards cold atmospheric plasma (CAP), which operates under atmospheric pressure and room temperature, as an emerging strategy for cancer treatment [1, 5–11]. Recent studies, including our own, have demonstrated that the synergistic efforts of reactive oxygen and nitrogen species (RONS, two primary constituents in CAP) can selectively induce cell death in various cancer types [12–17]. In comparison to traditional cancer therapies, such as chemotherapy and

†Xiaona Cao and Mo Chen contributed equally to this work.

*Correspondence:
Guojun Chen
guojun.chen@mcgill.ca
[1]Department of Biomedical Engineering, McGill University, Montreal, QC, Canada
[2]Rosalind & Morris Goodman Cancer Institute, McGill University, Montreal, QC, Canada
[3]School of Nursing, Tianjin Medical University, Tianjin, China
[4]Paul C Lauterbur Research Center for Biomedical Imaging, Shenzhen Institute of Advanced Technology, Chinese Academy of Sciences, Shenzhen, Guangdong, China
[5]Advanced Therapeutic Center, National Innovation Center for Advanced Medical Devices, Shenzhen, China

radiotherapy, CAP therapy boasts several distinct benefits. First, CAP therapy exclusively uses ionized gas for cancer treatment, eliminating the need for chemotherapy agents or radioactive medications, which often result in numerous undesirable side effects or harm to surrounding tissues [18–20]. Second, CAP leads to selective cancer cell deaths [13, 14]. Although the precise mechanism remains elusive, a plausible explanation is that cancer cells, driven by hypermetabolism, maintain a higher baseline oxidative level in contrast to normal cells. Consequently, the introduction of external oxidative agents, e.g. RONS in CAP, may easily reach the lethal oxidative threshold in cancer cells [12, 13, 21, 22]. These distinct advantages position CAP therapy as a promising alternative in the realm of cancer therapy.

Despite the unique merits of CAP therapy for cancer, the current CAP therapy regimen shows moderate cancer cell-killing efficacy, emphasizing a need to further enhance its therapeutic effect [23]. As mentioned earlier, RONS are the primary constituents in CAP that trigger cancer cell deaths by elevating cellular oxidative stress. RONS attack the lipid bilayer membrane leading lipid peroxidation and eventual cell death [24]. However, several intrinsic antioxidant defense systems exist in cells, such as the glutathione peroxidase 4 (GPX4) enzyme, which can catalyze the reduction of lipid peroxides. Rat sarcoma (RAS)-selective lethal 3 (RSL3), also known as a ferroptosis inducer, is a synthetic GPX4 inhibitor [25]. Thus, we hypothesize that a combination of CAP and RSL3 can show an additive antitumor effect.

In this study, we present a combined approach of CAP and RSL3 (CAP/RSL3) to enhance the efficacy of cancer therapy treatment (Fig. 1). RSL3 can inactivate GPX4, thereby sensitizing cancer cells to the oxidative stress induced by CAP and further enhancing cancer immunogenic cell death (ICD). Hydrophobic RSL3 was loaded in poly (ethylene glycol)-block-poly(lactide-co-glycolide) (PLGA-PEG) nanoparticles to improve its water solubility and in vivo stability. Tumor-associated antigens (TAAs) and damage-associated molecular patterns (DAMPs) are released to enhance the ability of dendritic cells (DCs) to present antigens to T cells, thereby facilitating the initiation and activation of T cells. Surprisingly, we demonstrated that CAP/RSL3 also effectively shifted tumor-associated macrophages (TAMs) from the M2 phenotype (pro-tumorigenicity) [26, 27] to the M1 phenotype (anti-tumorigenicity) [28, 29]. This polarization of macrophage increases macrophage engulfment of cancer cells, amplifies TAAs presentation to T cells, and boosts T-cell mediated anti-immunity.

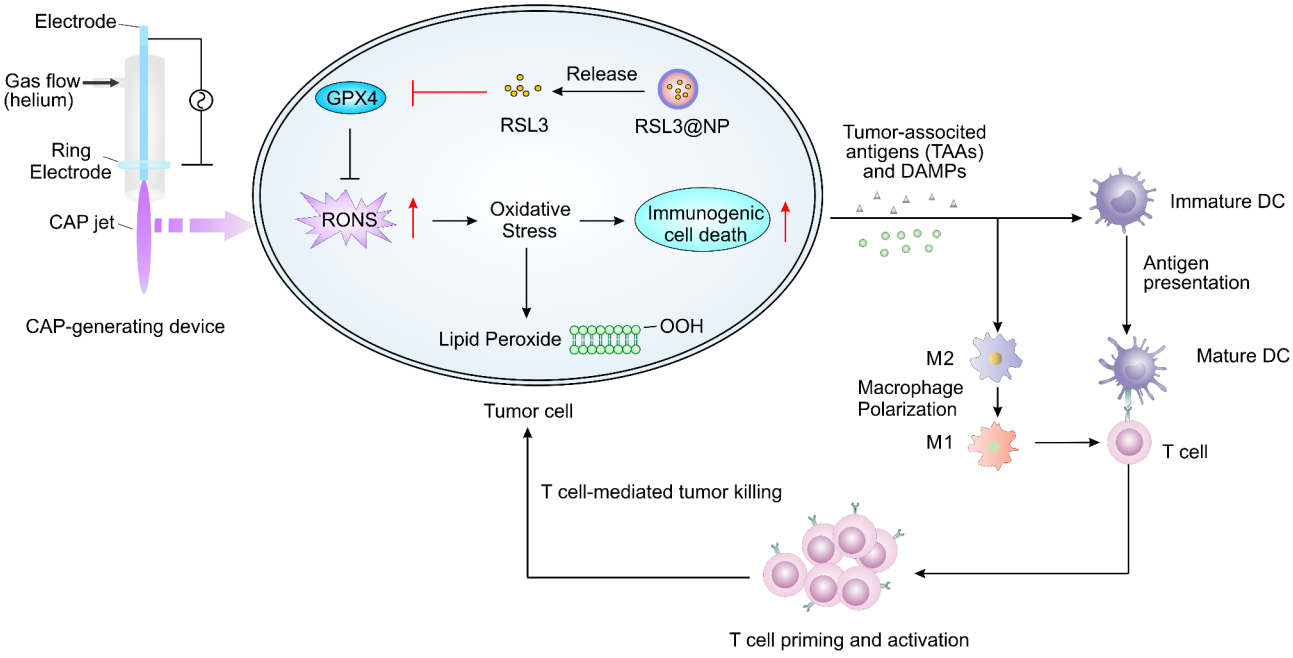

Fig. 1 Schematic of RSL3-loaded nanoparticles boosting CAP-mediated cancer immunotherapy *via* GPX4 inhibition. CAP treatment induces elevated oxidative stress in cancer cells, causing lipid peroxidation and thus cell deaths. However, the intrinsic antioxidant enzyme, GPX4, could recuse the oxidative stress-mediated cell death, thus suppressing the anti-tumor effect of CAP. RSL3, a GPX4 inhibitor, can inactivate GPX4 enzymes, thereby enhancing CAP-mediated ICD. The release of TAAs and DAMPs from dying cancer cells promotes the DCs maturation and TAMs polarization (from the M2 phenotype to the M1 phenotype) for enhanced TAAs presentation to T cells. T cell-mediated anti-tumor immune responses were then activated to combat tumor cells

Results and discussion

Characterization of RSL3-loaded PEG-PLGA nanoparticles (RSL3@NP)

RSL3, a synthetic GPX4 inhibitor, effectively decreased the expression level of GPX4 [30]. RSL3 is a hydrophobic drug [31], thus RSL3 was loaded in PEG-PLGA nanoparticles (RSL3@NP) to improve the water solubility [32]. The size of RSL3@NP is ~152 nm with a monodispersed and spherical morphology (Fig. 2A-C). The encapsulated efficiency and loading efficiency of RSL3@NP were 82% and 29%, respectively. As shown in Fig. 2D, about 48.5% of encapsulated RSL3 gradually released from RSL3@NP within 48 h.

RSL3@NP enhanced CAP-induced cell death *via* enhanced GPX4 inhibition in vitro

The CAP jet device (Fig. S1A) was assembled and utilized helium to produce CAP as previously described [12, 33]. The cytotoxicity of CAP varies in different cell lines (Figs. S1), and is CAP-time-dependent which is consistent with previous reports [12, 33]. CAP treatment increased the intracellular ROS and RNS in 4T1 breast cancer cells (Fig. 3A-B), and the addition of RSL3@NP further increased the ROS levels in cells. However, it is worth noting that RSL3@NP did not increase intracellular RNS levels. RSL3 is known to inhibit GPX4, and thus RSL3@NP effectively reduced the level of GPX4 in cells. Noticeably, GPX4 expression in cells was also seen to decrease after CAP treatment, and the combination of RSL3@NP and CAP exhibited an additive effect in GPX4 inhibition (Fig. 3C). As a result, the combination of RSL3@NP and CAP increased lipid peroxidation, a classic cellular response to the increased oxidative stress in 4T1 cells (Fig. 3D). Hence, we speculated that RSL3 could augment CAP-induced cancer cell deaths. Encouragingly, CAP/RSL3@NP significantly reduced cell viability in comparison to the mono-treatments (Fig. 3E, S1B-F, S2).

Combination of RSL3@NP and CAP activated anti-tumor immunity in vitro

Our previous data suggested that CAP can induce ICD and trigger T-cell-mediated anti-tumor immunity [13, 14]. Here, we investigated whether the combination of RSL3 and CAP could further amplify this anti-tumor effect. Three classic ICD markers, including calreticulin (CRT), adenosine triphosphate (ATP), and cytoplasmic localization of high mobility group protein B1 (HMGB1), were then assessed. CAP/RSL3@NP treatment effectively enhanced CRT exposure in 4T1 cells compared to CAP or RSL3@NP treatment alone (Fig. 3F). Increased ATP secretion (Fig. 3G) and HMGB1 translocation (Fig. 3H) were also observed in the CAP/RSL3@NP treatment group. These ICD markers can facilitate various stages of DCs involvement in the tumor microenvironment (TME), including the recruitment of immature DCs into the tumor environment (ATP-mediated), the engulfment of released TAAs by DCs (CRT-mediated), and the subsequent antigen presentation facilitated

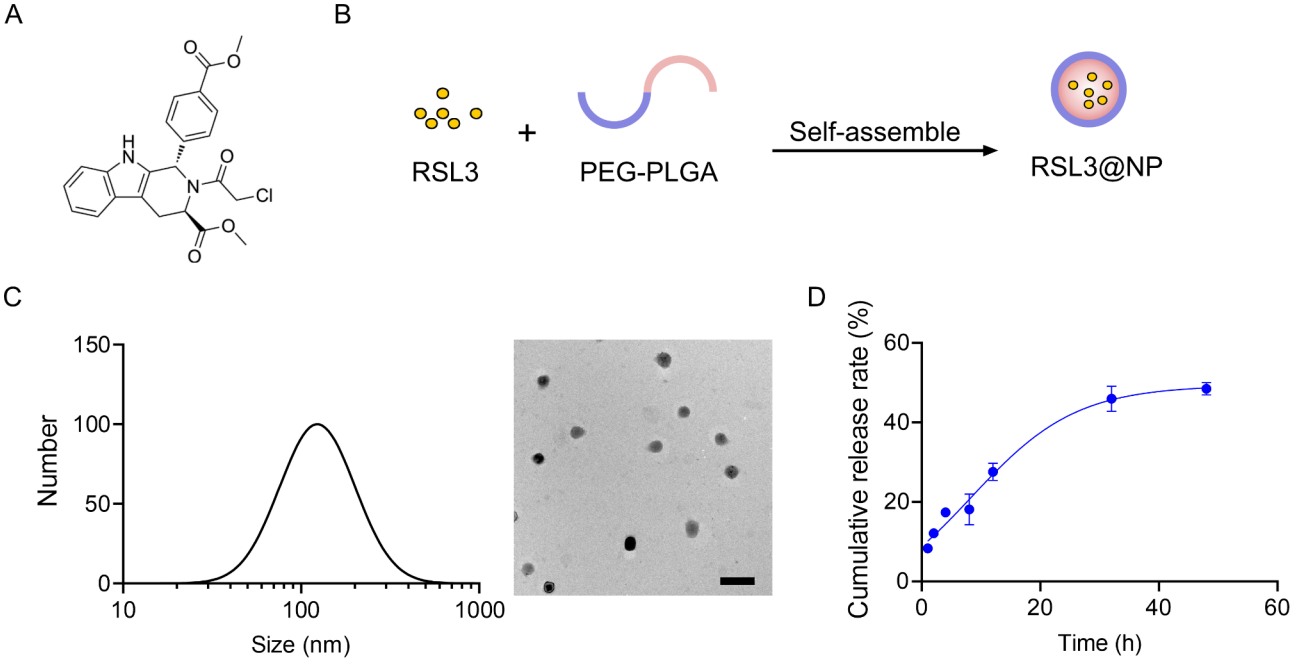

Fig. 2 Preparation and characterization of RSL3@NP. **(A)** Chemical structure of RSL3. **(B)** Preparation of RSL3@NP by self-assembly of PEG–PLGA copolymers. **(C)** Size and image of transmission electron microscopy (TEM) for RSL3@NPs (Scale bar = 500 nm). **(D)** The release profile of RSL3 from RSL3@NP. Data are presented as mean ± SD ($n = 3$)

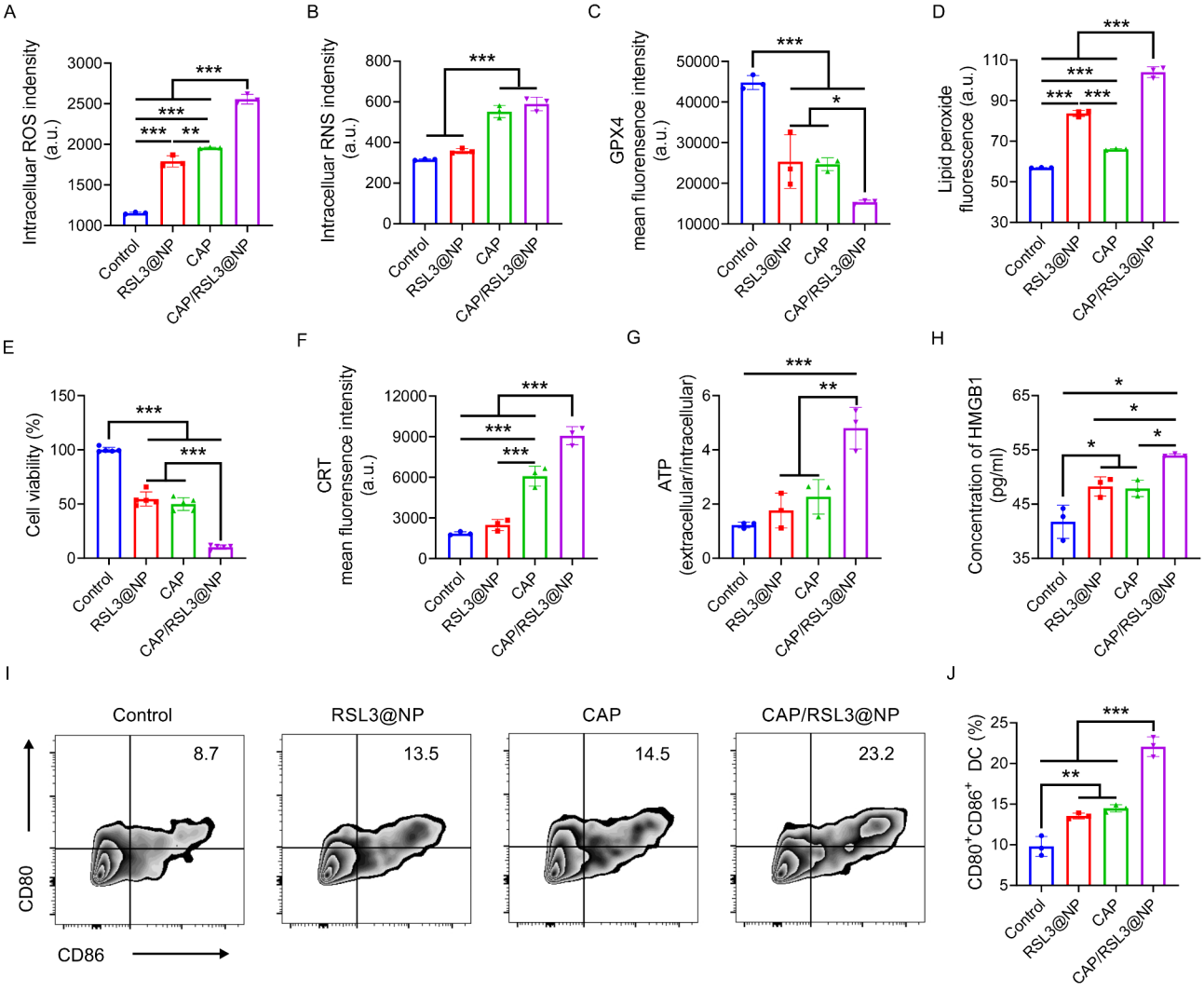

Fig. 3 RSL3@NP enhanced CAP-induced cell deaths *via* enhanced GPX4 inhibition and activated anti-tumor immunity in vitro. **(A)** ROS and **(B)** RNS levels in 4T1 cells after different treatments. **(C)** Flow cytometry quantification of GPX4 levels in 4T1 cells after different treatments. **(D)** Lipid peroxidation in 4T1 cells after different treatments. **(E)** Cell viability in 4T1 cells after different treatments. **(F)** Flow cytometry quantification of CRT levels in 4T1 cells after different treatments. **(G)** The ratio of ATP (extracellular/intracellular) in 4T1 cells after different treatments. **(H)** Concertration of HMGB1 in 4T1 cells after different treatments. **(I)** Flow cytometry plots and **(J)** quantification results of bone-marrow-derived DC maturation ($CD86^+CD80^+$) after coculturing with treated 4T1 cells. (Untreated cells were used as a control group; CAP-treatment time: 45s; RSL3@NP concentration (IC50): 400 nM). Data are presented as mean ± SD. Multiple comparisons were performed using one-way ANOVA and Tukey post-hoc tests. * $P < 0.05$, ** $P < 0.01$, *** $P < 0.001$

by HMGB1 [34–36]. Immature DCs, migrating to the tumor-draining lymph nodes, engage in the engulfment of TAAs and undergo maturation, ultimately presenting TAAs to T cells [37, 38]. To explore the immunological impacts of CAP/RSL3@NP on DC maturation, bone marrow-derived DCs were cocultured with CAP/RSL3@NP-treated cancer cells. A significant rise in matured DCs was observed (Fig. 3I-J, S3). As shown in Fig. S4A, the level of IL-6 in the combination group was significantly higher than in other groups, supporting the statement that CAP/RSL3@NP increased DC maturation. All these data strongly suggested that the CAP/RSL3@NP combination effectively initiated anti-tumor immune responses.

CAP/RSL3@NP combination suppressed the growth of tumor in vivo

The therapeutic intervention of the CAP/RSL3@NP treatment was further conducted in vivo. To facilitate the delivery of CAP to the tumor tissues, we also employed injectable Pluronic hydrogels as a scaffold to preserve RONS of CAP as reported in our recent paper [12, 39]. Briefly, Pluronic hydrogel is a thermo-sensitive injectable hydrogel and shows excellent capability to preserve and sustain the release of RONS, serving as an indirect CAP treatment method (Figs. S4B-C) [12, 33]. Here, RSL3@NP was co-loaded and delivered by the Pluronic gel (denoted as CAP/RSL3@NP@gel).

To confirm that CAP/RSL3@NP@gel can decrease the level of GPX4 in vivo, 4T1-bearing mice were intratumorally injected with RSL3@NP@gel, CAP@gel, or CAP/RSL3@NP@gel and tumor tissues were collected for GPX4 analysis (Fig. S4D). The level of GPX4 was significantly downregulated in the CAP/RSL3@NP@gel compared with other groups (Fig. 4A). We then evaluated the antitumor efficacy of CAP/RSL3@NP@gel treatment. In the same animal model, while mice treated with CAP@gel alone or RSL3@NP@gel demonstrated a degree of tumor control compared to the untreated mice, mice receiving CAP/RSL3@NP@gel exhibited the most significant impairment of tumor growth (Fig. 4B-C). Notably, there were no detectable changes in the macrostructure of major organs (Fig. 4D) or body weight loss of animals

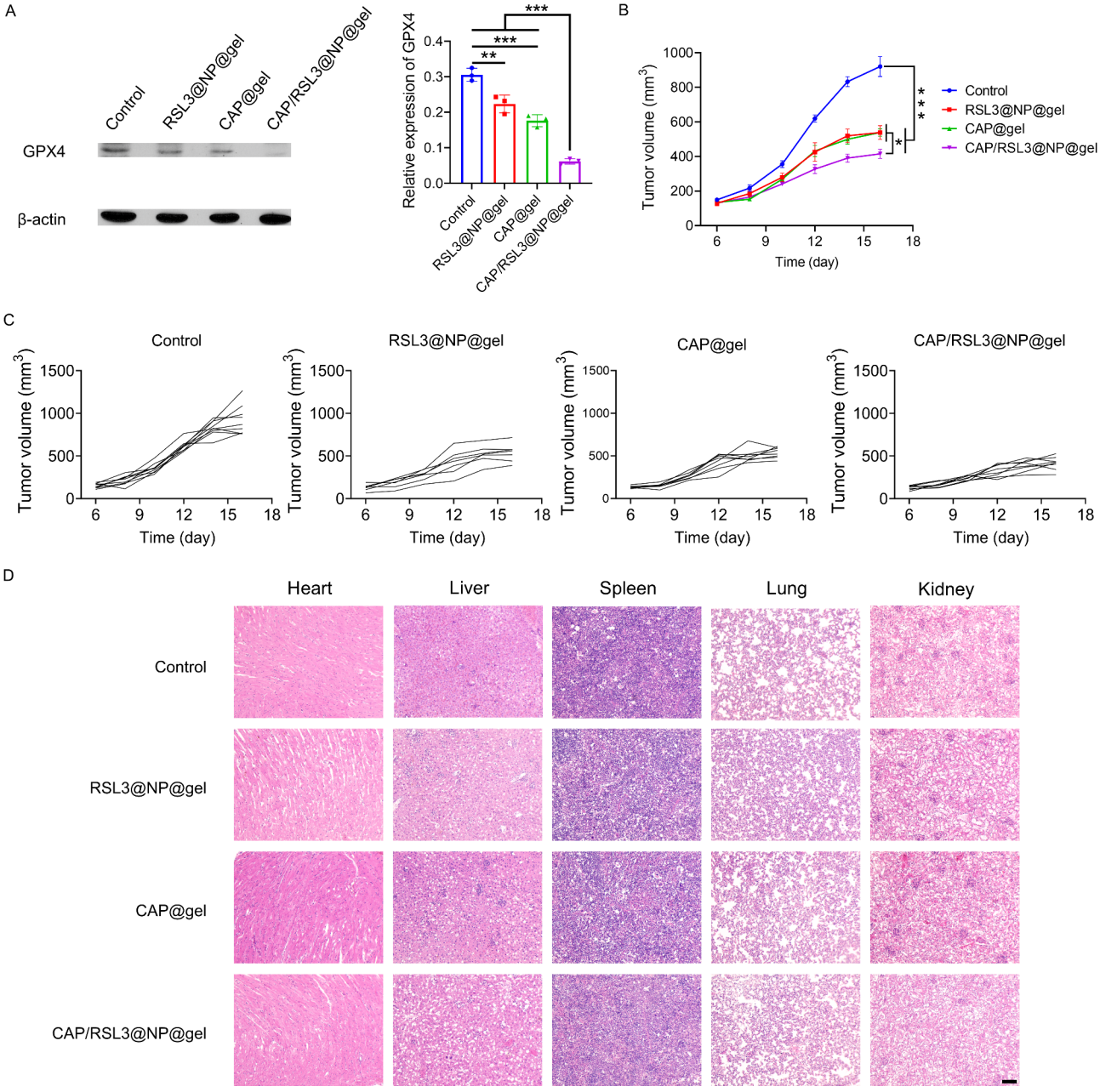

Fig. 4 CAP/RSL3@NP@gel treatment inhibited tumor growth in vivo. **(A)** Western blot and quantification of GPX4 in the tumor cells of RSL3@NP@gel (50 mg/kg), CAP@gel (10 min CAP-treated), or CAP/RSL3@NP@gel group. Data are presented as mean ± SD. **(B)** Average and **(C)** individual tumor growth kinetics in different groups after 5 injections every 2 days ($n = 9$ for the control group, $n = 7$ for the RSL3@NP@gel group, $n = 8$ for the other 2 groups). Data are shown as mean ± SEM. **(D)** H&E staining of major organs in different groups (Scale bar = 100 μm). Multiple comparisons were performed using one-way ANOVA and Tukey post-hoc tests. * $P < 0.05$, ** $P < 0.01$, *** $P < 0.001$

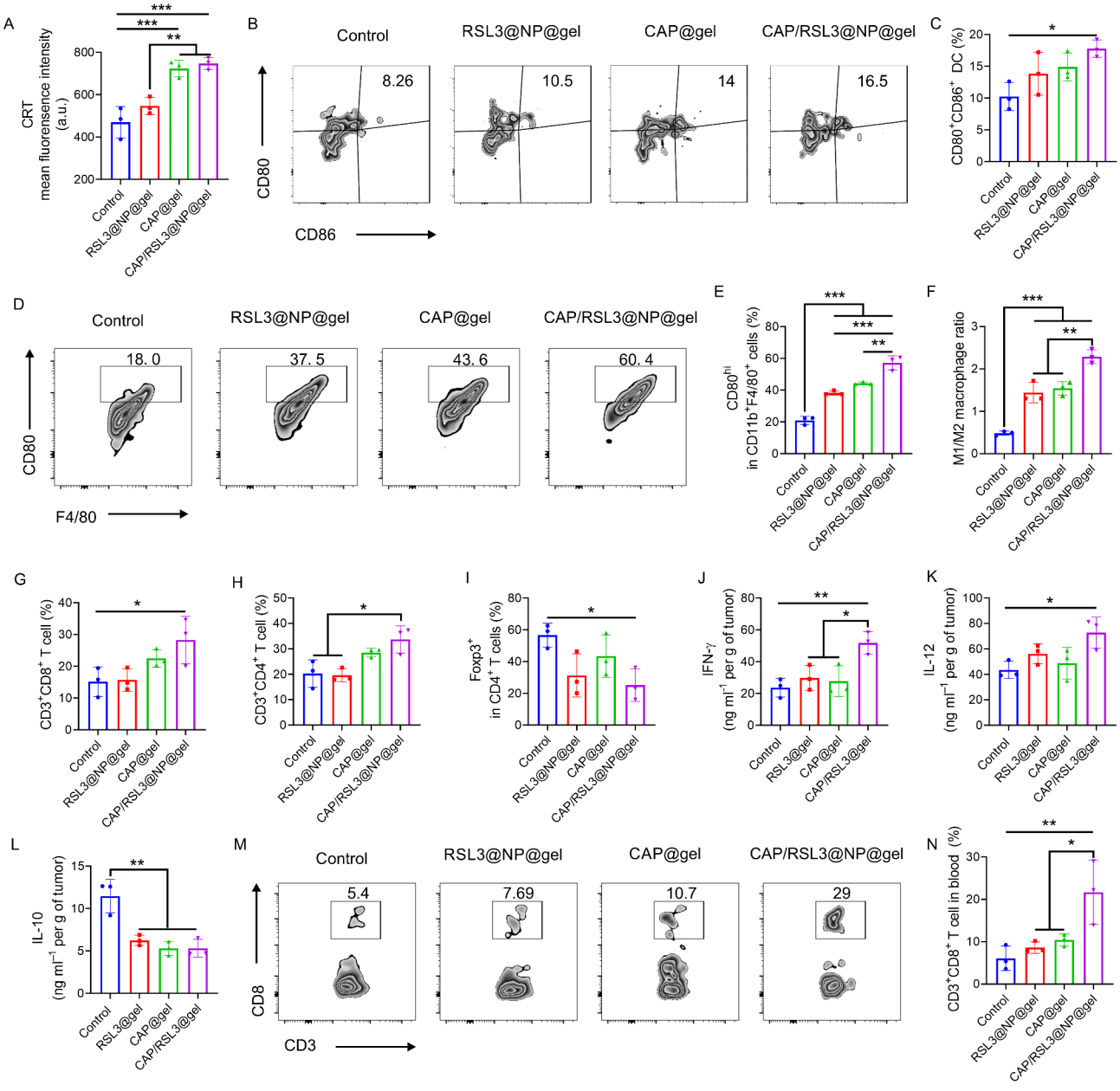

Fig. 5 CAP/RSL3@NP@gel treatment activated innate and adaptive antitumor immune responses in vivo. **(A)** Flow cytometry quantification of CRT on the tumor cells in different groups. **(B)** Flow cytometry plots and **(C)** quantification of mature DCs ($CD80^+CD86^+$ in $CD11c^+$ cells) within the tumors in different groups. **(D)** Flow cytometry plots and **(E)** quantification results of M1-like TAMs ($CD80^{hi}$ in $F4/80^+CD11b^+$ cells) within the tumors in different groups. **(F)** The ratio of M1/M2 TAMs within the tumors in different groups. **(G)** Flow cytometry quantification results within the tumors in different groups. Flow cytometry quantification results of **(H)** $CD3^+CD4^+$ T cells and **(I)** $Foxp3^+CD4^+$ T cells within the tumors in different groups. Intratumoral concentration of **(J)** IFN-γ, **(K)** IL-12, **(L)** IL-10 in mice of indicated treatments. **(M)** Flow cytometry plots and **(N)** quantification results of $CD3^+CD8^+$ T cells *in* the blood in different groups. Data are shown as mean ± SD (n = 3). Multiple comparisons were performed using one-way ANOVA and Tukey post-hoc tests. * $P < 0.05$, ** $P < 0.01$, *** $P < 0.001$

(Fig. S4E), confirming excellent biosafety of CAP/RSL3@NP@gel treatment.

CAP/RSL3@NP combination evoked T-cell-mediated antitumor immunity in vivo

Motivated by the enhanced therapeutic efficacy of CAP/RSL3@NP@gel in vivo, we evaluated the immunological responses associated with this treatment. Tumor and immune cells in the TME were assessed using flow cytometry. CRT exposure was increased on tumor cells in the CAP@gel and CAP/RSL3@NP@gel groups (Fig. 5A). Increased mature DCs were observed in the CAP/RSL3@NP@gel group (Fig. 5B-C). Meanwhile, we also checked the phenotype of TAMs, an important

innate immune cell that constitutes a substantial fraction (> 30%) of all the cells in the TME [40] and exhibits two distinct phenotypes with opposing immunological functions. M2-like TAMs, the dominant TAM phenotype in the TME, are often associated with tumor progression, metastases, and T cell suppression, while M1-like TAMs overexpress major histocompatibility complex class I and class II molecules (MHC-I and MHC-II) for effective antigen presentation [27, 29, 41]. Shifting M2 TAMs towards the M1 phenotype is conducive to anti-tumor immune responses. Surprisingly, the percentage of M1 TAMs was significantly elevated in the CAP/RSL3@NP@gel group (Fig. 5D-E), while the percentage of M2 TAMs was reduced in the treatment group (Figs. S5A-B). A clear increase in the ratio of M1/M2 macrophages was observed in the CAP/RSL3@NP@gel group (Fig. 5F). As previous reports, the release of DAMPs was positively correlated with polarization of M2-to-M1 TAM, thereby enhancing anti-tumor immune responses [27, 29, 41]. This macrophage polarization was also confirmed in vitro using bone marrow-derived macrophages (Figs. S5C-Q). More importantly, CAP/RSL3@NP@gel treatment increased the percentage of cytotoxic T lymphocytes ($CD3^+CD8^+$) and effector T lymphocytes ($CD3^+CD4^+$) within the TME (Fig. 5G-H, S6A). Notably, regulatory T cells (Tregs), a type of immunosuppressive immune cells, significantly decreased in the CAP/RSL3@NP@gel group (Fig. 5I, S6B). The alterations in cytokine secretion observed after CAP/RSL3@NP@gel treatment further substantiate the immune cell profiling results [41–43] as evidenced by the elevated levels of IFN-γ and IL-12 cytokine secretion and a lower level of IL-10 (Fig. 5J-L) [44]. Moreover, TIL ($CD3^+$) and cytotoxic ($CD3^+CD8^+$) T cells were significantly increased in the blood and spleens in CAP/RSL3@NP@gel treated mice (Fig. 5M-N, S6C-D, S7). Taken together, these findings suggest that CAP/RSL3@NP@gel treatment can effectively stimulate innate and adaptive immunity against tumors in vivo, supporting its superior anti-tumor behavior.

Conclusions and discussions

In this work, we reported that RSL3@NP can amplify the antitumor efficacy of CAP via enhanced GPX4 inhibition. Our results suggested that combining RSL3@NP with CAP led to increased cancer cell death both in vivo and in vitro. More importantly, injectable hydrogel-mediated delivery of RSL3@NPs and CAP elicited robust anti-tumor immunity, which included promoted DC maturation, the polarization of M2 to M1 phenotype TAMs, and enhanced T cell infiltration to tumor, which translated to improved anti-tumor therapeutic effects. Our findings also suggested the activation of a systemic T cell-mediated response by CAP/RSL3@NP@gel treatment, which holds promise for treating metastatic diseases and preventing disease recurrence.

While this proof-of-concept study highlights the effectiveness of combinational CAP/RSL3@NP@gel therapy, several critical research questions remain. First, the optimal timing for CAP/RSL3@NP@gel administration requires further investigation, as CAP and RSL3 exhibit therapeutic activity within different timeframes, which likely vary depending on the tumor type and stages of diseases. Second, beyond targeting the GPX pathway, inhibiting other intrinsic cellular antioxidant defense systems, such as catalase and superoxide dismutase, could also be considered for further therapeutical enhancement. Exploring combinations of various inhibitors presents a promising avenue, but comprehensive mechanistic studies are necessary to evaluate cell death modalities, immunogenic cell death (ICD) pathways, immune responses, and overall biosafety.

Methods and materials

Cell lines and animals

The murine 4T1 breast cancer cell line and the murine B16F10 melanoma cell line were obtained from the lab of Prof. Peter Siegel and the lab of Prof. Ian Watson at McGill University respectively. Cells were incubated in DMEM (Gibco, 11995065) with 10% FBS (Gibco, 12484028) and 1% penicillin/streptomycin (Gibco, 15140122) at 37 °C with 5% CO_2. Female BALB/c mice (7–8 weeks) were purchased from Charles River Laboratories. DMEM (Gibco, 21013024) was used in the CAP treatment. The animal studies were conducted by protocols approved by the Institutional Animal Care and Use Committee at the University of McGill, Canada.

Generation of CAP

The CAP device, featuring a needle electrode and a grounded ring electrode connected to a high-voltage transformer, was utilized for this research (Fig. S1A) [12, 33]. The gas used for the experiment was high-purity helium (99.996%) (Praxair, HE 5.0UH-K), with a flow rate of 8.5 L/min. The apparatus was operated at a current of ~ 3.5 A and a voltage of ~ 6 V. To produce CAP-treated solutions, the CAP jet was positioned 1 cm above the liquid surface (Fig. S1A).

Preparation and characterization of RSL3@NP

RSL3@NP was prepared by dissolving 200 mg PEG-PLGA (Sigma, 764825) and 100 mg RSL3 (AdooQ Bioscience, A15865) in 9 ml acetone. 50 ml dH_2O was added dropwise while stirring overnight. The sample was frozen in a -80 °C refrigerator and then lyophilized in the freezer dryer. The average particle size of RSL3@NP was measured by DLS (Brookhaven Instrument). The morphology of RSL3@NP was observed using transmission

electron microscopy (TEM). The unencapsulated RSL3 was removed with a 0.45 μm filter. The encapsulation of RSL3 in NP was analyzed by a high-performance liquid chromatography (HPLC) system (UltiMate 3000 HPLC) and a C18 column (NUCLEOSIL C18, 5 μm 15CM X 4.6 MM,). The mobile phase: acetonitrile water (50:50, v/v), constant flow rate: 1.0 mL/min. 10 μl of the solution were injected into the HPLC and then detected at a wavelength of 254 nm. The RSL3 loading efficiency was calculated according to the equation below: Loading efficiency (%) = $W_{RSL3\ in\ NPs}$ /W_{NPs} ×100%, encapsulation efficiency (%) = $W_{RSL3\ in\ NPs}$/$W_{RSL3\ fed}$ ×100%, where $W_{RSL3\ in\ NPs}$ represented the amount of RSL3 loaded in RSL3@NPs detected by HPLC. W_{NPs} represented the total weight of RSL3@NP; $W_{RSL3\ fed}$ represented the amount of RSL3 added in preparation of RSL3@NP.

Release of RSL3 from NPs

The RSL3@NP was prepared as described before. RSL3@NP was added to the dialysis bag (MW: 3500D) and incubated with 10 ml PBS release medium (PBS containing 5% SDS) at 37 °C and 100 rpm shaking. 100 μl of releasing media was collected at 1, 2, 4, 8, 12, 32, and 48 h for detection and substituted with the same amount of fresh release medium. The released RSL3 was detected using HPLC with the conditions described before.

Western blot

Protein extraction was using RIPA (Thermo Scientific, 89900) supplemented with protease inhibitors (Thermo Scientific, A32965) followed by sonication. Subsequently, the protein samples were separated through electrophoresis on a 12% SDS-PAGE gel and transferred onto a nitrocellulose membrane (Bio-Rad, 1620112) using electroblotting. The membrane was placed in 5% BSA TBST and incubated for 1 h at room temperature, then stained overnight with the antibody of GPX4 (Invitrogen, cat. no. PA5-19710) or β-actin (Invitrogen, PA516914) at 4 °C. Subsequently, the membranes were thoroughly washed and incubated with the HRP-conjugated secondary antibody (Invitrogen, 31460) for 1 h at room temperature. The bands were visualized using an ECL substrate (Thermo Scientific, 32209).

In vitro cell viability

Cancer cells (5×10^4/ml) were seeded into culture plates (96 wells) overnight. 4T1 cells were processed with the treatment of CAP (45 s), RSL3@NP (400 nM), and CAP/RSL3@NP for 24 h. 4T1 cells were processed with the treatment of CAP (45 s), RSL3 (75 nM), and CAP/RSL3 for 24 h. B16F10 cells were processed with the treatment of CAP (15 s), RSL3 (400 nM), and CAP/RSL3 for 24 h. Untreated cells were used as a control group. Cell viability was tested using the MTT assay. The cytotoxicity of RSL3@NP to T cell in vitro was analyzed by flow cytometry after staining with a LIVE/DEAD™ Viability/Cytotoxicity kit (ThermoFisher, L3224).

Intracellular ROS and RNS levels

Cancer cells (5×10^4/ml) were seeded into culture plates (24 wells) and cultured overnight. Cells were treated for 4 h and then stained with H2DCFDA (Invitrogen, D399) or DAF-FMDA (Invitrogen, D-23841) for 1 h. In the end, cell analysis was conducted using flow cytometry on the LSRFortessa system from BD.

Release of HMGB1

4T1 cells (5×10^3/well) were seeded in a 96-well plate for 24 h. 4T1 cells were treated under the different conditions of CAP (45 s), RSL3@NP (400 nM), and CAP/RSL3@NP. The culture medium was collected and analyzed with HMGB1 Elisa kit (Invitrogen, cat. no. EEL102).

Immunofluorescence

Cancer cells (5×10^4/ml) were seeded into culture plates (24 wells) and cultured overnight. The cells were treated for 12 h, and then they were fixed using 4% paraformaldehyde and permeabilized using 0.1% Triton for 10 min each. Following the blocking step in 5% BSA, cells were stained with HMGB1 primary antibody (Invitrogen, PA5-27378) and FITC secondary antibody (Invitrogen, F2765) at room temperature. Hoechst stain (Thermo Scientific, 62249) was used on the nuclei of cells. SlowFade Diamond Antifade Mountant (Invitrogen, S36972) was used to adhere coverslips to glass slides. Slides were examined by Zeiss (Observer. Z1) wide field microscopy).

The frozen sections of spleen were washed with PBS, and then blocked in 3% BSA for 1 h at room temperature. CD8a antibody (Invitrogen, cat. no. 42008182) and CD4 antibody (Invitrogen, cat. no. 50976682) were used to stain overnight at 4°C. Hoechst (Thermo Scientific, cat. no. 62249) was used to stain nuclei. The sections were preserved under SlowFade Diamond Antifade Mountant (Invitrogen, cat. no. S36972) and analyzed by widefield microscopy (Zeiss Observer. Z1).

In vitro CRT levels

Cancer cells (5×10^4/ml) were seeded into culture plates (24 wells) and cultured overnight. The next day, cells were treated under different conditions for 24 h (as described above). Afterward, cells were stained with CRT antibody (Invitrogen, PA3-900) and Alexa Fluor 555 antibody (Invitrogen, A21428). The BD LSRFortessa flow cytometry system was used for the subsequent analysis.

ATP release assay

Cancer cells (5×10^4/ml) were seeded into culture plates (96 wells) overnight. The cells were subjected to different

treatments for 24 h. A kit for ATP Determination (Invitrogen, A22066) was used to measure the luminescent signal of ATP in the cells and culture medium according to the guidelines provided by the manufacturer.

Dendritic cell maturation in vitro

Bone marrow-derived dendritic cells were isolated according to an established method [43]. The maturation of DCs was assessed utilizing a transwell culture system. The upper chamber of the transwell was cultured with cancer cells, while the lower chamber was cultured with bone marrow-derived DCs. Cancer cells were processed with the treatments for 6 h, then they were co-cultured with DCs for another 24 h. Following that, DCs were collected for staining with $CD80^+$ (BioLegend, 104723) and $CD86^+$ (BioLegend, 105008). The samples were subsequently analyzed using a BD LSRFortessa flow cytometer. IL-6 ELISA kit (BioLegend, Cat no. 431301) was utilized to measure the IL-6 levels in the culture medium for DCs.

Macrophage polarization in vitro

Bone marrow-derived macrophage cells were prepared as previous procedure [27, 45]. The macrophage polarization experiment was tested in a transwell assay. In the transwell, bone marrow-derived macrophages were cultured in the lower chamber, and cancer cells were grown in the upper chamber. Following a 6 h treatment, bone marrow-derived macrophages were co-cultured with cancer cells for an additional 24 h period. Subsequently, macrophages were collected for staining with $CD80^+$ (Invitrogen, 2381018) and $CD206^+$ (BioLegend, 141717), and were subsequently analyzed using a BD LSRFortessa flow cytometer.

Preparation of injectable gel

200 mg of Pluronic F-127 (Sigma, P2443-250G) was dissolved in 1 ml CAP-treated dH_2O to form CAP@gel at 4 °C. RSL3@NP@gel was prepared by loading RSL3@NP into Pluronic gel. CAP/RSL3@NP@gel was prepared by loading RSL3@NP into CAP@gel.

In vivo tumor models and treatment

To study the therapeutic effectiveness of CAP/RSL3@NP@gel, 1×10^6 4T1 cells were inoculated under the second left nipple of female BALB/c mice [39]. Mice with tumor sizes around 100 mm^3 were categorized into 4 groups ($n = 7$–9). CAP@gel, RSL3@NP@gel (50 mg/kg), or CAP/RSL3@NP@gel were injected intratumorally into mice-bearing tumors every two days for a total of five injections. The tumor volume was assessed using a digital caliper and was computed using the subsequent formula: $width^2 \times length \times 0.5$.

Immunological analysis

Tumors were collected after the last intratumoral injection. Tumor samples were cut and homogenized to form single cell suspensions with collagenase (Gibco, 17104019). Cell samples were stained with fluorescence-labeled antibodies: CD11c (BioLegend, 117310), CD86 (BioLegend, 105008), CD80 (BioLegend, 104723), F4/80 (BioLegend, 123116), CD206 (BioLegend, 141717), CD3 (BioLegend, 100204), CD4 (BioLegend, 100412), CD8 (BioLegend, 140408), Foxp3 (BioLegend, 126404). Blood samples were collected for the staining of CD3 (BioLegend, 100204), CD4 (BioLegend, 100412), and CD8 (BioLegend, 140408). The BD LSRFortessa flow cytometer was used to measure the stained cells.

Detecting cytokines in tumor tissue

Tumors were harvested and ultrasonic homogenized after the last injection. For detection of the intratumoral levels, ELISA kits of IL-12 (BioLegend, 433604), IFN-γ (BioLegend, 430801), and IL-10 (BioLegend, 431411) were utilized to measure.

Statistical analysis

Mean ± SD (standard deviation) was used to present results, except mean ± SEM (standard error of the mean) was used for the tumor growth curve. Multiple comparisons were performed using one-way ANOVA and Tukey post-hoc tests. All statistical analyses were carried out with the Prism software package (PRISM 5.0, GraphPad 2007). The threshold for statistical significance was $P < 0.05$.

Supplementary Information

The online version contains supplementary material available at https://doi.org/10.1186/s12951-025-03211-6.

Supplementary Material 1

Acknowledgements

The authors acknowledge McGill Life Science Complex Flow Cytometry Core, Histology Core, and the GCI Research Support team.

Author contributions

X.C. and M.C. contributed equally to this work. X.C.: Writing – review & editing, Writing – original draft, Methodology, Formal analysis. M.C.: Investigation, Formal analysis. T.F.: Formal analysis. Y.D.: Investigation. L.W.: Investigation. H.W.: Investigation. Z.C.: Writing – review & editing, Supervision, Formal analysis, Conceptualization. G.C.: Writing – review & editing, Writing – original draft, Supervision, Project administration, Funding acquisition, Formal analysis, Conceptualization.

Funding

This research was supported by McGill University's start-up package (to G.C.), CIHR grants (to G.C.), and CCS-Challenge Grants (to G.C.).

Data availability

Data is provided within the manuscript or supplementary information files.

Declarations

Ethics approval and consent to participate
The animal studies were conducted by protocols approved by the Institutional Animal Care and Use Committee at the University of McGill, Canada.

Consent for publication
The authors signed consent for publication.

Competing interests
The authors declare no competing interests.

Received: 1 May 2024 / Accepted: 10 February 2025
Published online: 24 February 2025

References

1. Chen Z, Chen G, Obenchain R, Zhang R, Bai F, Fang T, Wang H, Lu Y, Wirz RE, Gu Z. Cold atmospheric plasma delivery for biomedical applications. Mater Today. 2022;54:153–88.
2. Chen Z, Wirz RE. Cold Atmospheric plasma (CAP) technology and applications. Synthesis Lectures on Mechanical Engineering; 2021.
3. Nguyen HT, Bolouki N, Manga YB, Hsieh JH, Chuang EY, Chen CH. Novel gelatin–graphene oxide crosslinking induced by nonthermal atmospheric pressure plasma for alendronate delivery system. Plasma Processes Polym. 2020;17:2000110.
4. Satapathy MK, Manga YB, Ostrikov KK, Chiang W-H, Pandey A, Nyambat RL, Chuang B, Chen E-Y. Microplasma cross-linked graphene oxide-gelatin hydrogel for cartilage reconstructive surgery. ACS Appl Mater Interfaces. 2020;12:86–95.
5. Isbary G, Shimizu T, Li Y-F, Stolz W, Thomas HM, Morfill GE, Zimmermann JL. Cold atmospheric plasma devices for medical issues. Expert Rev Med Dev. 2013;10:367–77.
6. Tornin J, Labay C, Tampieri F, Ginebra M-P, Canal C. Evaluation of the effects of cold atmospheric plasma and plasma-treated liquids in cancer cell cultures. Nat Protoc. 2021;16:2826–50.
7. Busco G, Robert E, Chettouh-Hammas N, Pouvesle J-M, Grillon C. The emerging potential of cold atmospheric plasma in skin biology. Free Radic Biol Med. 2020;161:290–304.
8. Laroussi M, Kong MG, Morfill G, Stolz W. Plasma medicine: applications of low-temperature gas plasmas in medicine and biology. Cambridge University Press; 2012.
9. Shome D, von Woedtke T, Riedel K, Masur K. The HIPPO transducer YAP and its targets CTGF and Cyr61 drive a paracrine signalling in cold atmospheric plasma-mediated wound healing. Oxidative Med Cell Longev. 2020;2020(1):4910280.
10. Bolouki N, Hsu Y-N, Hsiao Y-C, Jheng P-R, Hsieh J-H, Chen H-L, Mansel BW, Yeh Y-Y, Chen Y-H, Lu C-X. Cold atmospheric plasma physically reinforced substances of platelets-laden photothermal-responsive methylcellulose complex restores burn wounds. Int J Biol Macromol. 2021;192:506–15.
11. Chen Y-H, Chuang E-Y, Jheng P-R, Hao P-C, Hsieh J-H, Chen H-L, Mansel BW, Yeh Y-Y, Lu C-X, Lee J-W, et al. Cold-atmospheric plasma augments functionalities of hybrid polymeric carriers regenerating chronic wounds: in vivo experiments. Mater Sci Engineering: C. 2021;131:112488.
12. Fang T, Cao X, Shen B, Chen Z, Chen G. Injectable cold atmospheric plasma-activated immunotherapeutic hydrogel for enhanced cancer treatment. Biomaterials. 2023;300:122189.
13. Chen G, Chen Z, Wen D, Wang Z, Li H, Zeng Y, Dotti G, Wirz RE, Gu Z. Transdermal cold atmospheric plasma-mediated immune checkpoint blockade therapy. Proceedings of the National Academy of Sciences 2020, 117:3687–3692.
14. Chen G, Chen Z, Wang Z, Obenchain R, Wen D, Li H, Wirz RE, Gu Z. Portable air-fed cold atmospheric plasma device for postsurgical cancer treatment. Sci Adv. 2021;7:eabg5686.
15. Zhang H, Xu S, Zhang J, Wang Z, Liu D, Guo L, Cheng C, Cheng Y, Xu D, Kong MG, et al. Plasma-activated thermosensitive biogel as an exogenous ROS carrier for post-surgical treatment of cancer. Biomaterials. 2021;276:121057.
16. Di Meo S, Reed TT, Venditti P, Victor VM. Role of ROS and RNS sources in physiological and pathological conditions. Oxidative Med Cell Longev. 2016;2016(1):1245049.
17. Lin AG, Xiang B, Merlino DJ, Baybutt TR, Sahu J, Fridman A, Snook AE, Miller V. Non-thermal plasma induces immunogenic cell death in vivo in murine CT26 colorectal tumors. OncoImmunology. 2018;7:e1484978.
18. Keidar M. Plasma for cancer treatment. Plasma Sources Sci Technol. 2015;24:033001.
19. Gurnett DA, Bhattacharjee A. Introduction to plasma physics: with space and laboratory applications. Cambridge University Press; 2005.
20. Lu X, Keidar M, Laroussi M, Choi E, Szili EJ, Ostrikov K. Transcutaneous plasma stress: from soft-matter models to living tissues. Mater Sci Engineering: R: Rep. 2019;138:36–59.
21. Trachootham D, Alexandre J, Huang P. Targeting cancer cells by ROS-mediated mechanisms: a radical therapeutic approach? Nat Rev Drug Discovery. 2009;8:579–91.
22. Schumacker PT. Reactive oxygen species in cancer cells: live by the sword, die by the sword. Cancer Cell. 2006;10:175–6.
23. Chen Y-H, Hsieh J-H, Wang I-T, Jheng P-R, Yeh Y-Y, Lee J-W, Bolouki N, Chuang E-Y. Transferred Cold Atmospheric plasma treatment on melanoma skin Cancer cells with/without catalase enzyme in Vitro. Appl Sci. 2021;11:6181.
24. Yang WS, SriRamaratnam R, Welsch ME, Shimada K, Skouta R, Viswanathan VS, Cheah JH, Clemons PA, Shamji AF, Clish CB, et al. Regulation of ferroptotic cancer cell death by GPX4. Cell. 2014;156:317–31.
25. Yang F, Xiao Y, Ding JH, Jin X, Ma D, Li DQ, Shi JX, Huang W, Wang YP, Jiang YZ, Shao ZM. Ferroptosis heterogeneity in triple-negative breast cancer reveals an innovative immunotherapy combination strategy. Cell Metab. 2023;35:84–e100108.
26. Noy R, Pollard JW. Tumor-associated macrophages: from mechanisms to therapy. Immunity. 2014;41:49–61.
27. Chen Q, Wang C, Zhang X, Chen G, Hu Q, Li H, Wang J, Wen D, Zhang Y, Lu Y, et al. In situ sprayed bioresponsive immunotherapeutic gel for post-surgical cancer treatment. Nat Nanotechnol. 2019;14:89–97.
28. Pittet MJ, Michielin O, Migliorini D. Clinical relevance of tumour-associated macrophages. Nat Reviews Clin Oncol. 2022;19:402–21.
29. Colegio OR, Chu N-Q, Szabo AL, Chu T, Rhebergen AM, Jairam V, Cyrus N, Brokowski CE, Eisenbarth SC, Phillips GM, et al. Functional polarization of tumour-associated macrophages by tumour-derived lactic acid. Nature. 2014;513:559–63.
30. Zhu X, Fu Z, Dutchak K, Arabzadeh A, Milette S, Steinberger J, Morin G, Monast A, Pilon V, Kong T, et al. Cotargeting CDK4/6 and BRD4 promotes senescence and ferroptosis sensitivity in Cancer. Cancer Res. 2024;84:1333–51.
31. Song R, Li T, Ye J, Sun F, Hou B, Saeed M, Gao J, Wang Y, Zhu Q, Xu Z. Acidity-activatable dynamic nanoparticles boosting ferroptotic cell death for immunotherapy of cancer. Adv Mater. 2021;33:2101155.
32. Zhang K, Tang X, Zhang J, Lu W, Lin X, Zhang Y, Tian B, Yang H, He H. PEG-PLGA copolymers: their structure and structure-influenced drug delivery applications. J Control Release. 2014;183:77–86.
33. Cao X, Fang T, Chen M, Ning T, Li J, Siegel PM, Park M, Chen Z, Chen G. Trehalose enhanced cold atmospheric plasma-mediated cancer treatment. Biomaterials. 2024;309:122582.
34. Kroemer G, Galluzzi L, Kepp O, Zitvogel L. Immunogenic cell death in Cancer Therapy. Annu Rev Immunol. 2013;31:51–72.
35. Eisenbarth SC. Dendritic cell subsets in T cell programming: location dictates function. Nat Rev Immunol. 2019;19:89–103.
36. Galluzzi L, Buqué A, Kepp O, Zitvogel L, Kroemer G. Immunogenic cell death in cancer and infectious disease. Nat Rev Immunol. 2017;17:97–111.
37. Banchereau J, Palucka AK. Dendritic cells as therapeutic vaccines against cancer. Nat Rev Immunol. 2005;5:296–306.
38. Leventhal DS, Gilmore DC, Berger JM, Nishi S, Lee V, Malchow S, Kline DE, Kline J, Vander Griend DJ, Huang H. Dendritic cells coordinate the development and homeostasis of organ-specific regulatory T cells. Immunity. 2016;44:847–59.
39. Fang T, Cao X, Wang L, Chen M, Deng Y, Chen G. Bioresponsive and immunotherapeutic nanomaterials to remodel tumor microenvironment for enhanced immune checkpoint blockade. Bioactive Mater. 2024;32:530–42.
40. Pathria P, Louis TL, Varner JA. Targeting tumor-associated macrophages in cancer. Trends Immunol. 2019;40:310–27.
41. Wen D, Liang T, Chen G, Li H, Wang Z, Wang J, Fu R, Han X, Ci T, Zhang Y. Adipocytes encapsulating Telratolimod Recruit and Polarize Tumor-Associated macrophages for Cancer Immunotherapy. Adv Sci 2022;10:2206001. https://doi.org/10.1002/advs.202206001
42. Korkaya H, Liu S, Wicha MS. Breast cancer stem cells, cytokine networks, and the tumor microenvironment. J Clin Investig. 2011;121:3804–9.

43. Chen Q, Xu L, Liang C, Wang C, Peng R, Liu Z. Photothermal therapy with immune-adjuvant nanoparticles together with checkpoint blockade for effective cancer immunotherapy. Nat Commun. 2016;7:1–13.
44. Brown JM, Recht L, Strober S. The Promise of Targeting macrophages in Cancer Therapy. Clin Cancer Res. 2017;23:3241–50.
45. Lee EJ, Nam GH, Lee NK, Kih M, Koh E, Kim YK, Hong Y, Kim S, Park SY, Jeong C. Nanocage-therapeutics prevailing phagocytosis and immunogenic cell death awakens immunity against cancer. Adv Mater. 2018;30:1705581.

Publisher's note